Non-equilibrium melting of colloidal crystals in confinement

E. Villanova-Vidal [a]; T. Palberg [a]; H. J. Schöpe [a]; H. Löwen [b]

[a] Institute of Physics, Johannes Gutenberg University, Staudinger Weg 7, D-55128 Mainz, Germany [b] Institute of Theoretical Physics II, Heinrich Heine Universität, Universitätsstrasse 1, D-40225 Düsseldorf, Germany

PLEASE SCROLL DOWN FOR ARTICLE

Taylor & Francis
Taylor & Francis Group

Non-equilibrium melting of colloidal crystals in confinement

E. Villanova-Vidal[a], T. Palberg[a]*, H.J. Schöpe[a] and H. Löwen[b]

[a]*Institute of Physics, Johannes Gutenberg University, Staudinger Weg 7, D-55128 Mainz, Germany;* [b]*Institute of Theoretical Physics II, Heinrich Heine Universität, Universitätsstrasse 1, D-40225 Düsseldorf, Germany*

A novel and flexible experiment is reported for investigation of the non-equilibrium melting behaviour of model crystals made from charged colloidal spheres. In a slit geometry, polycrystalline material formed in a low salt region is driven by hydrostatic pressure up an evolving gradient in salt concentration and melts at large salt concentration. Depending on particle and initial salt concentration, driving velocity and the local salt concentration, complex morphologic evolution is observed. Crystal–melt interface positions and the melting velocity are obtained quantitatively from time-resolved Bragg and polarisation microscopic measurements. A simple theoretical model predicts the interface to first advance, then for balanced drift and melting velocities to become stationary at a salt concentration larger than the equilibrium melting concentration. It also describes the relaxation of the interface to its equilibrium position in a stationary gradient after stopping the drive in different manners. The influence of the gradient strength on the resulting interface morphology and a shear-induced morphologic transition from polycrystalline to oriented single crystalline material before melting are discussed.

Keywords: confinement; zone melting; colloidal crystal; colloid; melting; microscopy; phase transition

1. Introduction

Consider a slab of ductile, low-melting material confined between chunks of larger rigidity and higher melting temperature. Subject this composite solid to a temperature gradient, which will partially melt the slab material and add a collinear pressure gradient. Depending on the sign of the latter, the slab material will either move down the temperature gradient and successively solidify or move up and successively melt. The former case is frequently encountered at die-casting or strip casting of alloys where intermediate semi-solid slurries are formed [1]; the latter is realised, for example, in zone melting, but may also occur in the perfusion of low melting rock material into other geological horizons or even in the process of magma intrusion into chambers from below [2]. Detailed knowledge about such phase transitions far from equilibrium conditions and at the same time influenced by restricted geometry is still poor, as such systems are notoriously inaccessible for

*Corresponding author. Email: Thomas.Palberg@uni-mainz.de

experiments and computationally extremely demanding due to the multiscale character of the problem. In the present contribution, we suggest how they can be investigated using a mesoscopic model system of charged colloidal crystals in confinement, which are simultaneously subjected to an external drive and a gradient in salt concentration.

Colloids in general offer a unique opportunity to precisely tailor particle interactions with experimental means, thus switching from repulsive to attractive, from short to long range, from spherically symmetric to dipolar or directed interactions [3]. Direct consequences of this tuneability are fascinating options to mimic atomic behaviour on a conveniently accessible mesoscopic scale. Hard sphere colloids in organic solvents form supercritical fluids, noble gas like, close packed crystals or fragile glasses [4], whereas hard spheres with added non-adsorbing polymers serve as weakly attractive model systems forming stable liquids and various ways of phase separation [5]. Like-charged spheres in, for example, water form fluids, crystals or amorphous solids [6,7], display metal-like elastic behaviour [8]. Here the spheres take the role of atoms and the counter-ions correspond to the (valence-) electrons. Finally, oppositely charged particles display a huge variety of salt structures [9,10]. Hence, a wide range of material classes is represented in the phase behaviour of colloids, and their equilibrium properties have been investigated in detail.

Recently, interest shifted to non-equilibrium processes with special focus on phase transitions kinetics and the influence of external fields [5,11–13]. In contrast to atomic systems, equilibrium melting is induced through a variation in interaction strength (e.g. via composition, concentration of particles and/or the amount of screening electrolyte) but not by an increase in temperature. The latter remains practically constant since the solvent acts as an effective heat sink. Still, the location of phase transitions is given by the ratio between thermal and interaction energy. Thus, several authors have demonstrated the existence of equilibrium fluid–melt interfaces in stationary gradients of different nature, including electrolyte strength, particle concentration or solvent composition [14,15]. Further, due to the soft matter nature of colloidal crystals (yield moduli of a few Pa only) application of external electric or magnetic fields [16,17] or mechanical stress [18–21] (both often in combination with confinement or the presence of rigid surfaces) are well suited to induce both melting and freezing or manipulate the systems morphology during solidification. Thus, the issue of non-equilibrium phase transitions can also be addressed in a very flexible way.

In the present paper, we present the outline and preliminary results on a new kind of experiment. With this we go beyond previous work in several points. First we study melting rather than crystallisation. Here much less is known about the mechanisms involved to start and dominate the phase transition kinetics in an anisotropic environment. In contrast to the rich literature on the quantitative kinetics of crystal growth [5,11,12], even a qualitative parameterisation of melting kinetics is missing completely. Still open issues are, for example, the role of dislocations, grain boundaries and free surfaces [22–25] favouring either randomly distributed global or local initiation of the melting process. Secondly, stationary gradients of interaction strength have been introduced in various ways [14,15]. We combine here such a gradient with an external pressure difference, and thus for

the first time move the solid with respect to the gradient. Finally, previous work has focused on bulk situations. Here, we explicitly study the influence of the induced motion within the parallel wall confinement on the phase transition process.

The paper is organised as follows. We first briefly introduce the sample and the experimental set-up including a characterisation of the gradient formation and the pressure driven crystal motion. After giving an overview on the complex temporal evolution of the samples, we present exemplary quantitative measurements of melting kinetics. A theoretical model is established in the next section, which is able to predict the interfacial velocity in the presence of a constant drive and after stopping the drive. We finally turn to a description and discussion of the peculiar morphological differences observed for different gradient strengths and the morphologic transition observed in strong gradients and in the presence of shear along a solid wall. We conclude with a short discussion of the scope and range of our approach.

2. Experimental

2.1. *Sample cell*

Experiments were performed in a commercial Microlife cell (Hecht, Germany), as shown in Figure 1. Two reservoirs are connected by a thin slit. The reservoirs contain approximately 1.5 ml of suspension; the actual parallel plate measuring chamber spans 47 mm in the x direction and has a width $y = 7.5$ mm and a height $z = 500\,\mu$m. One reservoir contains ca. 1 ml of mixed bed ion exchange resin (IEX; Amberlite, Rohm & Haas, France). The cell is filled with suspension from a peristaltic conditioning circuit, where the desired number density of particles and the initial salt concentration were adjusted. Typically the suspension is deionised, but saturated with gaseous CO_2. The cell is then disconnected from the circuit and tightly sealed with screw caps. For technical reasons an air bubble remains under each lid.

The cell conveniently meets the two main requirements of our experiment: the possibility to maintain a stationary gradient in salt concentration along the cell and
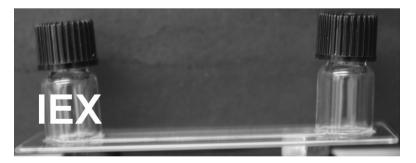

Figure 1. Sample cell. The reservoirs contain approximately 3 ml of suspension; the actual parallel plate measuring chamber spans 47 mm in the x direction, has a width $= 7.5$ mm and a height $z = 500\,\mu$m. In the filled state, one reservoir contains ca. 1 ml of mixed bed ion exchange resin (IEX).

the possibility to generate a pressure difference between the two reservoirs causing a slow flow of the suspension through the cell.

2.2. *Formation of a stationary salt gradient*

As only one of the reservoirs contains the IEX, the initially homogeneous salt concentration evolves into a gradient along the measuring chamber. The evolution of the gradient is not directly accessible. Therefore, reference experiments were performed in a quartz cell of rectangular cross-section ($L \times W \times D = 150 \times 10 \times 1 \, mm^3$) connecting a reservoir filled with IEX with a second one without IEX. Here the local ion concentration was determined from either conductance measurements (performed with a set of 11 equispaced pairs of platinum electrodes placed at the small sides of the cell) or by photometry. We observed that the initial salt gradient was quite steep, close to the IEX then extended and flattened. Linearity was typically reached within one to two weeks, slightly varying with initial salt concentration. This evolution was found to be independent of the type of salt chosen (CO_2, NaCl, Uranin). Using dissolved CO_2 as salt source has the advantage of keeping the reservoir salt concentration constant at a well defined level through the dissociation equilibrium $CO_2 + 2H_2O \leftrightarrow HCO_3^- + H_3OH^+$. Over a length of 47 mm the salt concentration drops linearly from $c = c_0 = 1.1 \times 10^{-5} \, mol \, l^{-1}$ in the IEX-free reservoir with a CO_2 saturated state to $c = 2 \times 10^{-7} \, mol \, l^{-1}$ (from the self-dissociation of water) at the IEX-containing reservoir.

This gradient is stable until either all dissolved CO_2 has dissociated or the IEX becomes exhausted. Starting from CO_2 saturated conditions, the former typically happens on a time scale of half a year, whereas with approx. 1 ml of IEX the latter occurs within two to three months. Therefore, the location of the melting salt concentration c_M for a given particle number density is precisely determined for a time interval of say two weeks to two months. A second even stronger gradient is present above the IEX towards that reservoir's gas bubble. The average salinity in this reservoir therefore is considerably smaller than in the other. Steeper gradients can be adjusted in the measuring chamber from elevated initial salt concentrations and will also pertain over weeks to months depending on the amount of added salt, the quantity of IEX present and the size of the reservoir.

2.3. *Generation of a pressure gradient*

Upon filling, the sample is saturated with dissolved CO_2 but does not contain dissociated CO_2. Thus, in a first process, CO_2 dissociates leading to $c = c_0$. In the IEX-free reservoir, the dissociated CO_2 is slowly removed towards the IEX side across the cell. It is replenished by freshly dissociating CO_2, which in turn is replaced by gas from the air bubble in the lid. Hence, there is a slight drop in the gas pressure on the IEX-free side. On the IEX side, an additional process is present. Due to the reduced average salinity the solubility of CO_2 drops [26] and neutral gas starts forming small bubbles adding to the gas bubble in the IEX side lid. Thus, here a net pressure increase occurs. The situation is sketched in Figure 2. To restore the pressure balance, a very slow flow of suspension towards the IEX-free side occurs.

Figure 2. Realisation of a pressure drive. One reservoir of the cell is filled with IEX. The IEX exchanges carbonate ions from dissociated CO_2 for hydroxyl ions re-combining with protons to water. At locally reduced salinity in the left reservoir, the lowered solubility of CO_2 leads to degassing into the air bubble. At the opposite reservoir, the salinity stays constant buffered by the reservoir of CO_2 in the air bubble, ready to dissolve and dissociate. A gas pressure difference is thus created exerting a force on the suspension, which drives it through the narrow part of the cell connecting the reservoirs.

We checked that the motion is slow enough to not affect the salt gradient between the fixed positions of IEX and IEX-free reservoir. This may occur, when the suspension porosity becomes low and is a well-known effect, e.g. in sedimentation or in electrophoresis [27]. In our case, the volume fraction is in the order of 1% or below and the solvent drains freely through the crystallites. Hence, the suspension is pushed up the salt gradient.

The pressure difference cannot be measured directly. Rather its qualitative behaviour as a function of time was inferred from the induced motion of the sample through the flat part of the cell. Here, we exploited the effect that crystalline suspensions mostly showed a plug flow, which allowed a convenient determination of the position of individual crystallites as a function of time from sequences of micrographs taken on the sample. Figure 3a gives a graphic definition of measurable quantities. The positions $X_C(t)$ of individual crystals at similar x-position but differing y-position can be monitored as a function of time. The positions $M(t)$ and $L(t)$ of the (curved) boundary between the two morphologies and of the (curved) crystal melt interface are determined as averages over the entire cell width, when only small curvatures are present. For strongly curved interfaces we preferred to first measure crystal and interface positions along several of the clearly visible stream lines, then calculate and average $W(t)$. The average extension of the WC region is obtained from $W(t) = L(t) = M(t)$. Position measurements at individual times contain a comparably large uncertainty (typically $\pm 100 \, \mu m$) due to the irregular fluctuations (presumably caused by coalescence of gas bubbles) superimposed on the continuous drift. Therefore, average propagation velocities were inferred from measurements performed over some hundred minutes.

By changing the initial CO_2 content, the size of the reservoirs, the amount of IEX and the size of the air bubbles, the pressure difference and the temporal evolution of the pressure difference and thus the drift velocity can be varied. For standard conditions (1 ml IEX, CO_2 saturated suspension with no salt added) drift velocities of 0.5–$5 \, \mu m \, min^{-1}$ were generated. Larger velocities could be obtained using an elevated initial salt concentration. Slower drifts were realised if the IEX-free side was left
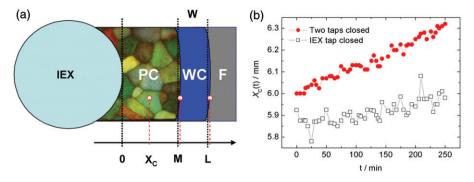
Figure 3. (a) Definition of lengths to be measured in X direction: X_C: drifting crystal position; M: position of the morphological boundary between polycrystalline region (PC) and wall crystal region (WC); L: position of the crystal/melt interface. For flat interfaces y-averaged values were used (dotted black lines); for curved interfaces measurements were restricted to y-positions belonging to the same stream line (red dotted lines). (b) Comparison of drifts as observed for a sample at $n = 12\,\mu m^{-3}$ under different conditions. Upper curve: initial salt concentration $20\,\mu M$ NaCl and both reservoirs tightly sealed; lower curve: no added salt, CO_2 saturation and the non-IEX side reservoir open to ambient air. Note the lower drift velocity and the increased fluctuations in the lower curve due to decreased pneumatic damping.

open to air. An example is shown in Figure 3a, comparing the latter two cases. Typically, a roughly constant average drift velocity was obtained within one hour correlating with the time scale of deionisation in the IEX reservoir. The drift typically pertained over a few weeks. It then slowly decreased to finally vanish when the degassing process, feeding the pressure difference, ceased.

2.4. *Sample and initial sample conditioning*

The highly charged, small latex spheres (effective charge from elasticity measurements $Z_{eff} = 582 \pm 18$, diameter from ultracentrifugation $2a = 122\,nm$, standard deviation $\sigma = 0.02$) used in this work were synthesised by surfactant-free emulsion polymerisation and were a kind gift of BASF, Ludwigshafen. Samples were prepared from pre-cleaned stock suspensions, filtered and stored over IEX. Samples were left in contact with air to obtain a thorough saturation with air-borne CO_2. For further conditioning they were then filled into a closed, peristaltically driven preparation cycle [28] connected to the measuring cell. The desired number densities were adjusted by dilution with doubly distilled, but CO_2 saturated water under control of static light scattering. Number densities n were chosen to be above the equilibrium melting density at deionised conditions ($n_M(c=0) \approx 0.1\,\mu m^{-3}$). The suspension was then deionised again to remove the dissociated CO_2. During conditioning, a metastable shear melt existed throughout the circuit and cell. The cell was then disconnected, and, if desired, a small amount of salt solution was mixed into the suspension. After introducing the IEX on one side, the cell was sealed with air tight screw caps. This defines $t = 0$. For observation, the cell was mounted on the stage of an inverted microscope (IRB, Leica, Wetzlar, Germany) and monitored with a high resolution CCD camera. Two observation modes were regularly
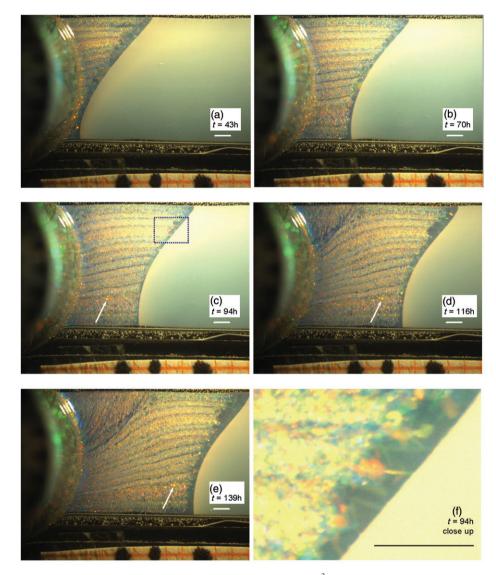
Figure 4. (a–e) Micrographs for a suspension at $n = 12\,\mu m^{-3}$ and initial salt concentration of $20\,\mu M$ NaCl for different times t after filling. Images were taken close to the IEX side of the cell. The cell sides are just visible at the top and bottom. (a) $t = 43\,h$, (b) $t = 70\,h$, (c) $t = 94\,h$, (d) $t = 116\,h$ and (e) $t = 139\,h$. The white scale bar is 1 mm, crystal extension may further be estimated from the orange square raster at the bottom. The white arrow marks an individual crystal position used to determine $X_C(t)$. Note that the crystal approaches the crystal melt interface as time proceeds. Note further the stream lines in the polycrystalline part of the advancing solid and the variation of the thickness of the darker, wall crystal region. (f) Magnification of the marked upper boundary region in (c), scale bar 1 mm, which compares the smoothness of the crystal melt interface to the roughness of the morphologic transition boundary.

applied: polarisation and Bragg microscopy [12]. Data were stored in a computer and image processed to quantify sample structure, morphology and motion.

3. Melting experiments

Since the observed phenomena occur on time scales of 1–2 months, a large parameter space had to be covered in order to obtain a general picture. Typically two samples were prepared at identical conditions to exclude preparation artefacts, and typically both showed qualitatively very similar results. The statistics of this overview are therefore of restricted quality, but systematic trends can safely be identified and are discussed in Section 3.1. For selected samples, additional quantitative measurements were performed to study the kinetics in more detail. Even for qualitatively similar pairs, the kinetics were found to differ considerably, depending on the amounts of CO_2 initially present and of IEX added. Hence, in Section 3.2 we shall demonstrate the principle of quantitative measurements on one selected sample without generalising the obtained numbers to other sets of experimental parameters.

3.1. *General observations*

We investigated some 120 samples with no added salt or with an initial salt concentration of 5–50 μM NaCl. All samples readily crystallised within a few seconds after sealing and placing the cell on the microscope stage. Large n samples formed polycrystalline solids, and low n samples formed large single crystals via heterogeneous nucleation at the container walls. For large n and low salt initial concentrations these crystals were found to be stable. For low n samples and large n large salt samples, the crystallites melted again after a few ten minutes, showing a characteristic Swiss cheese morphology indicative of a homogeneous release of ions during CO_2 dissociation (an example is shown in Figure 6a). The melting time scale further agrees well with the results of reference experiments on the conductance of pure water. There, a homogeneous concentration of $c = c_0$ was typically reached within an hour.

Independent of the initial melting stage, the IEX immediately starts to remove salt next to the IEX reservoir. This locally leads to a steep gradient of salt concentration, which extends and flattens with time. In this gradient, starting next to the IEX the molten samples re-crystallised. The recrystallised volume increased with time displaying a sharp boundary to the melt state. For combinations of n and c_0 close to the equilibrium melting conditions, the crystal melt boundary advanced though the complete cell. Only for combinations corresponding to an equilibrium fluid, the crystal-melt interface advanced to a position well accessible in the optical part. For CO_2 saturated initial conditions, this was observed for $3 \, \mu m^{-3} \leq n \leq 15 \, \mu m^{-3}$, for elevated salt concentrations this occurred at correspondingly larger n.

The speed of the advancing interface is determined by both the drift velocity and the melting or growth velocity at the crystal-melt interface. This latter velocity is determined by the local salt concentration and hence coupled to the temporal development of the salt gradient. Also the shape of the advancing interface is

determined this way and variations of either drift velocity or salt concentration in y-direction may lead to a curved interface. In practice, interfaces were frequently observed to be sharp and only show a mild symmetric variation by less than 2 mm across the complete y-direction. Other samples, however, showed considerable curvature and differential advancement at different y-positions. In some of these, we could discriminate bent rows of crystallites emerging from the IEX. Resembling the flow traces of glaciers, the crystal production and drift history is captured in such stream lines of crystals. On the other side, in some cases, the interface advancement is of different speed for different y-positions, while at the same time the drift velocity is stationary across the whole crystal. This indicates a variation of the salt concentration in y-direction. Also the observation, that even late stage equilibrated interfaces often remain curved, supports this suggestion. Typical examples of both effects are shown in Figures 4a–e for a suspension of $n = 12 \, \mu m^{-3}$ and an initial salt concentration of 20 μM NaCl.

The overall temporal evolution in general is quite complex and differs in details for different initial conditions. Still, a standard scenario can be identified for the interface forming systems: after initial melting and formation of a crystal melt interface close to the IEX, the advancement of the interface continues for some 10 to 30 days, depending on the initial conditions. During this time, the salt gradient is fully established, and after some 15 to 30 days the drift gradually ceases. The interface position then either becomes stationary or shows a very slow retreat, to again stabilise after one or two weeks. The final position is found to be stable for an extended time, until the IEX becomes exhausted. For a typical volume of IEX of 1.5 ml this takes about two to three months. After that the crystal melt interface recedes and the crystals disintegrate until the sample is completely molten. With our set-up we may observe both the melting of crystals pushed up the gradient, when the melting salt concentration is beyond the crystal melt interface, and the columnar growth of crystals, when the melting salt concentration is ahead of the crystal melt interface. Hence, the two main processes of zone melting are covered. In addition, we may also access an equilibrated melt-crystal interface over several weeks.

3.2. *Melting kinetics*

In this section, we show how to extract quantitative information on the kinetics from sequences of microscopic images. In Figures 4a–d, we show images of a suspension at $n = 12 \, \mu m^{-3}$ and an initial salt concentration of 20 μM taken near the IEX-containing reservoir taken during the first five days. In Figures 5a–c, we show the same suspension for much later times. Here the complete cell is shown. In both figures the IEX side is to the left. In Figures 4a–d, one may clearly distinguish the extensions of crystalline and fluid regions and in a qualitative way see their motion.

From sample images, the drifting crystal positions and the interface location were determined within stream lines with a temporal resolution of 10 min. Results for $t_{start} \approx 50 \, h$ are shown in Figures 6a–c for the interfacial position, $L(t)$, the drifting crystal position, $X_C(t)$ and their difference. From these measurements, the velocity of crystal melt interfacial advancement, v_{front}, the drift velocity, v_{drift}, and the velocity, v, can be inferred by least square linear fits. Obviously, the crystal drift velocity is much
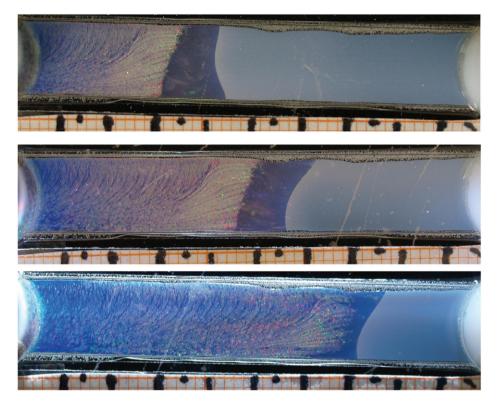
Figure 5. As in Figure 4, but now showing the complete cell for times of $t = 12$ days, $t = 22$ days and $t = 29$ days (from top to bottom). The scale is seen from the orange, 1 mm square raster at the bottom. Note the backward advancement of the morphologic boundary, presumably caused by vanishing of small crystals in the stream lines in favour of the large wall crystals.

larger than the interfacial velocity. Hence, $v = -45\,\mu\mathrm{m\,h^{-1}}$ is negative and a *melting* velocity. The crystal melts as it is pushed up the gradient.

Comparison of the linear fit with the data in Figure 6a shows that the interface position $L(K)$ still advances quite linearly in time after two days ($t_{\mathrm{start}} = 49.72\,\mathrm{h}$). Figure 6b reveals that the drift already slows down a bit, as does the melting velocity in Figure 6c. Several days later the interfacial velocity slows noticeably. This can be seen in Figure 6d, where we show the interfacial position of our sample with a temporal resolution of one day over the entire measurement. For comparison, we also include the data set for another sample at $n = 6\,\mu\mathrm{m^{-3}}$ and no salt added. Here an indication of relaxation behaviour is seen.

4. Theoretical model

In a first approach to a theoretical description, we make some simplifying assumptions. First we assume a fully developed stationary gradient, which is not perturbed by the advancing crystal. Second, we assume the drift velocity to be
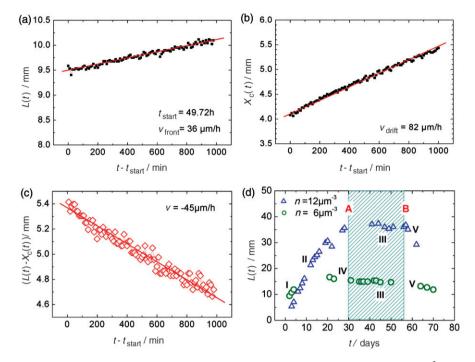
Figure 6. (Colour online). Characteristic quantities for the sample at $n = 12\,\mu m^{-3}$ and an initial added salt concentration of $20\,\mu M$ shown in Figures 4 and 5. (a) Interfacial position $L(t)$. (b) Drifting crystal positions $X_C(t)$. Positions were determined in 10 min intervals taken simultaneously for some 10^3 min. Velocities indicated were derived from linear fits to the position data. (c) Evolution of the difference between $L(t)$ and $X_C(t)$ as a function of time. The difference decreases, showing that the crystals melt at the interface. (d) The extension of the solid region $L(t)$ over the complete measurement for two samples of concentrations as indicated. Experiments on the sample of lower density were performed without added salt. The slowing approach of a stationary interfacial position is clearly visible. After presenting a stationary interface over more than a month (between A and B), the position recedes again due to exhaustion of the IEX. Roman numerals mark the different stages of the temporal evolution: I, initial melting; II, advance of the interface; III, stationary interface; V, degradation. An additional relaxation stage (IV) seems to be visible in the data of a sample with smaller concentration and no added salt ($n = 6\,\mu m^{-3}$), but this stage in general was found much less clearly distinguishable and reproducible.

constant in time. Finally, we focus on the case of balanced drift and melting velocities to stabilise the interfacial position. That is, we investigate the case of an overheated crystal. All these assumptions may be released later on, e.g. by including the temporal development of the drift velocity and the gradient and allowing for crystal growth.

In order to establish a simple theoretical framework to classify and describe the zone melting behaviour, we assume a Wilson–Frenkel law [29,30] for the modulus of the interface velocity v in terms of the dimensionless "overheating" $\Delta\mu/k_B T = (\mu - \mu_M)/k_B T$ [31][1]

$$v = v_\infty(1 - \exp(-\Delta\mu/\kappa_B T)), \qquad (1)$$

where v_∞ is the modulus of the limiting velocity at extreme overheatings, μ is the actual chemical potential of the colloids and μ_M denotes the colloid chemical potential at fluid–solid coexistence. The colloidal particles interact via a Yukawa pair potential [32]

$$V(r) = V_0 \exp(-\kappa r)/r, \tag{2}$$

with $V_0 = Z_{\mathrm{eff}}^2 k_{\mathrm{B}} T \lambda_{\mathrm{B}}$ and the screening parameter defined via $\kappa^2 = 4\pi\lambda_{\mathrm{B}}(Z_{\mathrm{eff}}\, n + 1000 N_{\mathrm{A}} c)$, r denoting the interparticle distance and $k_{\mathrm{B}} T$ the thermal energy. Z_{eff} is the colloidal effective charge number and $\lambda_{\mathrm{B}} = 7.8$ Å is the Bjerrum length, n denotes the colloidal number density, c the molar salt concentration and N_{A} is Avogadro's number. The Yukawa potential provides a reasonable description of the interaction [33,34] and the freezing and melting boundaries [7,35–37] for charged-stabilised colloidal suspensions. We then derive an approximate expression for $\Delta\mu/k_{\mathrm{B}} T$ by mapping the Yukawa interaction potential onto a soft inverse power potential $\tilde{U}(r) = U_0\,(\sigma/r)^4$. In this substitute potential, the dimensionless quantity $\Delta\mu/k_{\mathrm{B}} T$ can only depend on differences in the dimensionless coupling strength $\Gamma = U_0\sigma^4\rho^{4/3}/k_{\mathrm{B}} T$ such that $\Delta\mu/k_{\mathrm{B}} T = \Delta\Gamma$. We map the potential $\tilde{U}(r)$ onto $V(r)$ by requiring that

$$\tilde{U}(d_{NN}) = V(d_{NN}), \tag{3}$$

where $d_{NN} = \sqrt{3} \times 2^{-2/3} \times n^{-1/3}$ is the nearest neighbour distance in the bcc crystal. Different salt concentrations lead to a variation of κ and hence they map onto a different Γ [38][2].

In a prescribed salt gradient dc/dx, the crystal–melt interface at position L corresponds to a chemical potential difference of

$$\Delta\mu/k_{\mathrm{B}} T = \alpha(L - L_0), \tag{4}$$

with L_0 denoting the interface position in equilibrium at zero velocity and

$$\alpha = 4\pi\lambda_{\mathrm{B}}^2 Z_{\mathrm{eff}}^2 \exp(-\kappa d_{\mathrm{NN}})\frac{dn_s}{dx}\frac{1}{\kappa}. \tag{5}$$

Now we prescribe a time-dependent drift velocity $v_D(t)$. The actual interface velocity dL/dt then is a difference of the imposed drift $v_D(t)$ and the melting interface velocity given by Equation (1):

$$dL/dt = v_D(t) - v_\infty(1 - \exp(-\alpha(L - L_0))), \tag{6}$$

which can be cast into the reduced form

$$dy/d\tilde{t} = g(\tilde{t}) - (1 - \exp(-y)), \tag{7}$$

with the reduced time $\tilde{t} = \alpha v_\infty t$, and $y(\tilde{t}) = \alpha(L(\tilde{t}/\alpha v_\infty) - L_0)$ and $g(\tilde{t}) = v_D(\tilde{t}/\alpha v_\infty)/v_\infty$. This differential equation can be solved for constant drift velocities v_D and the solution is summarised as follows:

$$y(\tilde{t}) = \ln(\exp(A\tilde{t})(A \exp y(0) + 1) - 1/A, \tag{8}$$

where $A = v_D/v_\infty - 1$. For $v_D < v_\infty$, this implies that the growth saturates at $y(\tilde{t} \to \infty) = -\ln(1 - v_D/v_\infty)$ and this plateau value is reached exponentially in (reduced) time with a decay constant of $1/A$. For $v_D > v_\infty$, on the other hand, $y(\tilde{t})$
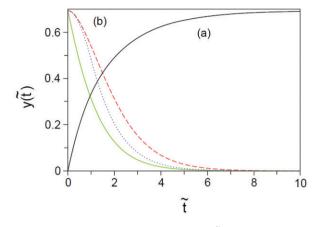
Figure 7. (Colour online). Reduced interface position, $y(\tilde{t})$, versus reduced time $\tilde{t}$ for various time-dependent drift velocities as obtained by a numerical solution of the non-linear differential Equation (7) for (a) $y(0) = 0$ and $g(\tilde{t}) = \Theta(\tilde{t})/2$; (b) $y(0) = \ln 2$ after releasing g from $g = 1/2$ to zero as (i) $g(\tilde{t}) = \exp(-\tilde{t})/2$ (broken line), (ii) $g(\tilde{t}) = (1 - \tilde{t})/2$ for $0 < \tilde{t} < 1$ and zero elsewhere (dotted line), (iii) $g(\tilde{t}) = \Theta(-\tilde{t})/2$ (full line). Here $\Theta(\tilde{t})$ denotes the unit step function.

diverges linearly in time as $y(\tilde{t}) \approx (v_D/v_\infty - 1)\tilde{t}$. Finally, for the border case where the drift velocity coincides with the limiting velocity, $v_D = v_\infty$, we find an interesting logarithmic interfacial growth in time given by

$$y(\tilde{t}) = \ln(\tilde{t} + \exp y(0)). \tag{9}$$

For a general $v_D(t)$ there are only numerical solutions for the non-linear differential equation, Equation (7). We have plotted the interface position as a function of time for different time-dependent drift velocities in Figure 7. When the drift is switched on, the interface velocity first follows the drift but is then reduced by melting until the steady state is approached at balanced drift and melting velocity.

At first sight, this behaviour appears rather similar to the evolution of the interface position in Figure 6d. There are, however, some interesting differences. First, the experimental drift velocity is continuously reduced after two to three weeks. Hence the stationary interfacial position of the experiment (Stage III), is located closer than theoretically predicted or even at the equilibrium value. Second, at later stages there is a variation of the interface position by both melting and growth, which in addition varies with y-direction. This can be seen by closer inspection of Figures 5a and b. Focussing on the position of prominent features in the transition between the multicoloured polycrystalline region and the dark blue wall crystal region, one sees no variation in these features over a period of ten days. At the same time, however the lower part of the crystal melt interface has retreated, whereas the upper has advanced. Thus the wall crystal melts at some but grows at other y-positions, pointing at a variation of the salt concentration also across the cell. A y-direction variation of the salt gradient is difficult to implement without precise knowledge of the experimental boundary conditions. Here for the time being one has to restrict the quantitative

comparison to cases of flat interfaces. Third, the presence of crystal growth in the experiments was not addressed here, but is covered by the model. Growth occurs when in the symmetric Wilson–Frenkel law (Equation (1)) chemical potential differences of opposite sign are used.

On the other side, the theoretically modelled situation of balanced drift and melting velocity is experimentally realised during the transition from stage I to stage II. During this period, the drift is large and constant and the gradient is still steep. The interface first still recedes, but then for many hours the interface stays at approximately constant position and the microscopic analysis shows balanced velocities. Later, as the gradient evolves and the salt concentration at the interface decreases, the melting velocity has reduced below the drift velocity and the interface advances.

A first extension of the simple case discussed above was performed in a study of the relaxation from the stationary (velocity balanced) state to the equilibrium state after releasing the drift. Results are also shown in Figure 7. Here three different cases corresponding to an instantaneous turn off of drift and to a linear and exponential decrease of drift are plotted. The relaxation time of the drift is mixing with the ultimate relaxation time αv_∞ of the interface. This curve in principle corresponds to the relaxation part of the $n = 6 \, \mu m^{-3}$ sample shown in the experimental data of Figure 8. Unfortunately, at the present stage, the uncertainty in the experimental parameters is still too large to perform a detailed quantitative comparison by estimating the different time scales using, for example, Equation (5) or to assess the logarithmic interface growth predicted for the border case in Equation (9). This is left for future studies. We finally remark that close to equilibrium the non-linear differential equation, Equation (7), can be linearised ($\exp(-y) \approx 1 - y$) and then the analytical solution becomes
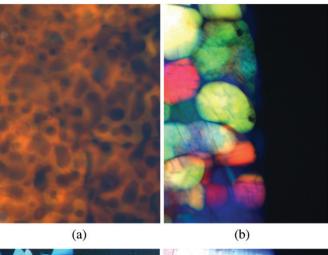
$$y(\tilde{t}) = y(0) \exp(-\tilde{t}) + \int_0^{\tilde{t}} dx' \, (g(x') \exp(x' - \tilde{t}), \tag{10}$$

which can be used for an asymptotic study close to equilibrium if the drift is released.

To summarise the theoretical part: a simple theory assuming a Wilson–Frenkel law makes predictions for the time-dependent interface position in a salt gradient for a given constant drift velocity and can be used to study trends when other quantities are varied such as salt gradient, colloid effective charge and different time-dependent prescribed drift velocities. One further prediction is that, if the drift is released, the interface position approaches its equilibrium value exponentially in time. The associated decay time is αv_∞. Future extensions of the theory may conveniently be included. Future work will explicitly include the combined time dependence of drift and salt gradient to cover the experimental evolution of the interface position in more detail.

5. Morphologic development

Two points concerning the sample morphology are of special interest. First, we observe rather different morphologies upon melting under different circumstances. Second, with a drift present, the polycrystalline material shows a morphologic transition before melting, which can be viewed as shear assisted alignment.
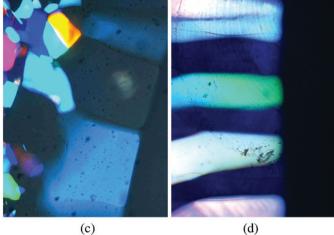
Figure 8. Different morphologies obtained by melting under different boundary conditions. (a) Swiss cheese morphology frequently observed during initial melting by homogeneously released carbonate (image height ca. 8 mm). (b) Polycrystals slowly advancing and melting in a shallow gradient resemble a beach of pebble stones. In an extended coexistence region, these melt inward (image height ca. 4.6 mm). (c) Polycrystals in a strong drift, approaching the crystal melt interface in a steep gradient. Before melting they transform to large wall crystals of like crystallographic orientation. The wall crystals melt with straight sharp boundaries, showing kinks at their grain boundaries (image height ca. 5 mm). (d) Columnar crystals grown in the absence of a drift (both taps open) and slowly melting in a moderate gradient as the carbonate concentration increases and showing extended kinks (image height ca. 5 mm).

We first turn to the morphological differences observed under different conditions of melting. Concerning the initial melting stage, it is caused by a more or less homogeneous release of carbonate ions. Presumably for most of the cell no strong gradients in salt concentration are present. In this case, we observe a peculiar Swiss cheese like structure of the melting crystals. An example is shown in Figure 8a. Here white light illumination was used in combination with Bragg

microscopy adjusted to meet the (111) reflection, leading to the characteristic rainbow like colour distribution for different angles of incidence. Quite a different morphology is seen when for low n samples the polycrystalline material produced on the IEX side reaches the crystal–melt interface. Here the crystals melt starting from their grain boundaries, yielding a pebble like appearance of the sample shown in Figure 8b obtained from polarisation microscopy. At particle densities larger than $5.5\,\mu m^{-3}$, a wall crystal region appears close to the crystal melt interface. It is formed from the polycrystalline material. In this case of melting of oriented wall crystals in a gradient, a sharp interface is observed. Presence of several crystallites with quite parallel grain boundaries gives the crystal melt interface a characteristic teeth-like appearance (Figure 8c). For the most part, the crystal the interface is straight, but at the grain boundaries between different crystals one clearly observes the presence of kinks. Finally, in the absence of drift (both taps open) recrystallisation occurs by growth of columnar crystals, some of these also showing the characteristic colour of preferred orientation with the densest packed plane parallel to the cell wall, but others being oriented differently. The image in Figure 8d gives an example for a low n case, where, like in Figure 8b, the crystal melt interface is again more bent.

The main difference between the different situations is given by the steepness of the local salt gradient. Swiss cheese morphologies appear for vanishing gradients (cf. Figure 8a), while straight fronts appear for fast melting in a steep and straight gradient (Figure 8c). Grain boundaries widening to pebblish morphologies with intact crystal interior as well as grooves entering at the grain boundaries mediate between these extremes. Here a moderate gradient is present, which may initiate two effects: first, salt may possibly enter the crystalline region better along the less ordered grain boundaries; second, the grain boundaries may have a lower melting point than the well ordered crystals. Both give rise to a realisation of the coexistence region (between c_F and c_M) with roundish crystals embedded in the coexisting fluid. The peculiar appearance, as either pebbles or fingers, relates to the initial crystal morphology after formation (polycrystalline or columnar). All of these interface morphologies have been observed before: the pebblish appearance of polycrystals at coexistence was first noticed some time ago [39] and columns have also been reported, e.g. by Yamanaka et al. [14]. Even Swiss cheese structures have been observed in very carefully sealed, gradient-free cells to evolve over several hours [25]. In addition, recent studies using confocal microscopy showed that in nearly hard sphere crystals pre-melting occurs at defects, dislocations or grain boundaries providing a convenient way of starting the melt process [24]. The comparison made here, however, combines observations made on one species of charged spheres subjected to different kinds of gradients and thus allows assessment of the solitary findings of previous work under a new common point of view.

Second, we have observed that after a few mm of drift, the polycrystalline material transforms to rather uniformly oriented monolithic wall crystals of tooth-like to columnar morphology. In Figures 5 and 8c, the multicoloured polycrystalline region is clearly separated from the crystal–melt interface by a dark blue region of wall-based crystals. Also the boundary of the morphological transition is slightly bent and initially follows the shape of the crystal–melt interface. The boundary is

smooth on a large scale. But it is rough on a scale of several crystallites, as the transition often affects several neighbouring crystals at the same time or advances several crystals deep into the polycrystal following a stream line (cf. Figures 4 and 5). Concerning individual crystals, we have observed wall crystals emerging from coalescence of two or more polycrystals. We have seen individual crystals flip colour as a whole but also sometimes seen a straight boundary to propagate through a crystal. The latter case may be some extreme case of coarsening, simply enlarging the volume of the adjacent wall crystal and minimising its surface. Coarsening is also present in the polycrystalline material as it is pushed up the gradient and enters regions of elevated salt concentration. There is, however, an important difference to normal bulk coarsening in a quiescent sample where random orientation of crystallites is retained. In our case, due to the fluctuations of the gas pressure, our coarsening suspension is sheared by a superposition of steady and oscillatory shear, with the largest shear rates at the walls. Additional scattering experiments reveal that beyond the zone of large polycrystals all wall crystals are oriented alike with the densest packed plane parallel to the confining walls and the densest packed direction parallel to the drift velocity. A similar orienting influence of an externally applied shear was found by computer simulations of sheared bilayers in [40,41] and experimentally observed in re-crystallisation experiments after directed shear melting [42] or even in continuous oscillatory shear [43]. Following these authors, also in our case the orientation of the dense packed planes is steered by the wall orientation, while further shear stress minimisation occurs by orienting the easy shear direction parallel to the drift direction. As we are working in a gradient of salt concentration, the interaction strength also decreases upon approaching the melting transition. Both shear modulus and yield modulus are directly related to the latter [44]. In the low salt polycrystalline region, the solid may still resist plastic deformation by shear and simple strains. At increased screening, however, it yields and is reoriented.

6. Conclusions

We have reported a novel versatile set-up to study non-equilibrium melting of charged sphere colloidal crystals either subjected to a spatially homogeneous increase in salt concentration or pushed up a gradient in salt concentration, such that a competition between drift velocity and thermodynamically controlled melting velocity occurs. In addition, equilibrated interfaces are also obtained in a stationary salt gradient. We have demonstrated how kinetic measurements yield the involved velocities, and established a simple model to predict the advancement of the interface. Whereas most observations are still in a preliminary state, we feel that the approach taken may in future significantly enrich our understanding of the melt process of colloidal model crystals. A number of interesting questions may be addressed. For example, small quantities of an additional species could be added to study the role of impurities in melting and their fate after re-solidification (crystal purification). Samples prepared close to the bcc-fcc-fluid triple point will complement previous studies on study phase selection during crystallisation by others during melting with or without external fields applied.

Also, the studies could be extended to the melting of twinned bcc wall crystals obtained after directed shear melting at low *n*. From the technical point of view, one may replace the pressure drive by a piezomechanic drive to obtain a programmable drift and realise situations better comparable to theoretical predictions. Theory as well may be considerably extended to include a temporal variation of salt gradients and drift velocities. We therefore think to have presented a very flexible new concept to approach melting studies with model crystals. Moreover, equilibrated interfaces may also be of great interest. In particular, an analysis of the radius of curvature of the equilibrated grooves of neighbouring crystals possibly offers an approach to fluid-crystal interfacial tensions, hardly accessible in other experiments.

In addition to charged sphere model crystals, it will also be of interest to study crystals of other interactions, e.g. hard sphere crystals [4], ionic crystals of oppositely charged spheres [9,10] or crystals forming in attractive systems [5]. In mixtures, additional segregation phenomena may be expected. Also such systems should be equally well suited for studies of their melting kinetics and mechanisms in gradients, close to confining walls and under shear.

All of these questions, however, are of great interest to other scientific communities involved with non-equilibrium thermal processing of materials, e.g. metallurgy or geology. Here our approach bears the perspective of flexibly adjusting the boundary conditions to model closely related situations known from atomic matter. For instance, the pressure drive mimics fluctuations inevitable e.g. in die or strip casting and presumably also in geologic processes. Furthermore, we have shown that the gradient characteristics directly influence the resulting melting morphology and that the simultaneous presence of shear and confining walls can significantly alter the melting process. Similar effects are also expected for atomic systems of spherically symmetric interactions. On the other side, it would be interesting to study whether the Swiss cheese melting morphology can have a counter-part in atomic systems or is a colloid specific phenomenon. With our approach we hope to have stimulated fruitful discussions on the reported physical phenomena and demonstrated the potential of colloidal models to address non-equilibrium issues.

Notes

1. It is still unclear whether in the solid–fluid coexistence region there is steady-state interfacial growth; see, for example, the discussions in [31] and the experimental findings of [42].
2. A different mapping procedure was used by M.S. Ripol, C.F. Tejero and M. Baus [38].

References

[1] M. Ferry, *Direct Strip Casting of Metals and Alloys: Processing, Microstructure and Properties*, CRC Press, Boca Raton, 2006.

[2] C. Wicks, W. Thatcher, D. Dzurisin and J. Svarc, Nature 440 (2006) p.72.

[3] A. Yethiraj, Soft Matter 3 (2007) p.1099.

[4] P. Bartlett and W.v. Megen, in *Granular Matter*, A. Mehta, ed., Springer, New York, 1994, p.195.

[5] V.J. Anderson and H.N.W. Lekkerkerker, Nature 416 (2002) p.811.

[6] E.B. Sirota, H.D. Ou-Yang, S.K. Sinha, P.M. Chaikin, J.D. Axe and Y. Fujii, Phys. Rev. Lett. 62 (1989) p.1524.

[7] M.O. Robbins, K. Kremer and G.S. Grest, J. Chem. Phys. 88 (1988) p.3286.

[8] D. Reinke, H. Stark, H.-H. von Grünberg, A.B. Schofield, G. Maret and U. Gasser, Phys. Rev. Lett. 98 (2007) p.0380301.

[9] M.E. Leunissen, C.G. Christova1, A.-P. Hynninen, C.P. Royall, A.I. Campbell, A. Imhof, M. Dijkstra1, R. van Roij and A. van Blaaderen, Nature 437 (2005) p.235.

[10] E.V. Shevchenko, D.V. Talapin, S. O'Brien and C.B. Murray, J. Am. Chem. Soc. 127 (2005) p.8741.

[11] B.J. Ackerson (ed.), Phase Transitions 21 (1990) p.73.

[12] T. Palberg, J. Phys. Condens. Matter 11 (1999) p.R323.

[13] H. Löwen, J. Phys. Condens. Matter 13 (2001) p.R415.

[14] J. Yamanaka, N. Murai, Y. Iwayama, M. Yonese, K. Ito and T. Sawada, J. Am. Chem. Soc. 126 (2004) p.7156.

[15] A. Toyotama, J. Yamanaka, M. Yonese, T. Sawada and F. Uchida, J. Am. Chem. Soc. 129 (2007) p.3044.

[16] S.O. Lumsdon, E.W. Kaler and O.D. Velev, Langmuir 20 (2004) p.2108.

[17] L.E. Helseth, H.Z. Wen, J.P. Hansen, T.H. Johansen, P. Heinig and T.M. Fischer, Langmuir 20 (2004) p.7323.

[18] B.J. Ackerson, Physica A 128 (1983) p.221.

[19] J. Vermant and M.J. Solomon, J. Phys. Condens. Matter 17 (2005) p.R187.

[20] W.D. Dozier and P.M. Chaikin, J. Phys. France 43 (1982) p.843.

[21] T. Palberg, W. Mönch, J. Schwarz and P. Leiderer, J. Chem. Phys. 102 (1995) p.5082.

[22] C. Murray, D.H. van Winkle and R. Wenk, Phase Transitions 21 (1990) p.75.

[23] Z.Z. Gu, A. Fujishima and O. Sato, J. Am. Chem. Soc. 122 (2000) p.12387.

[24] A.M. Alsayed, M.F. Islam, J. Zhang, P.J. Collings and A.G. Yodh, Science 309 (2005) p.1207.

[25] H. Yoshida, J. Yamanaka, T. Koga, T. Koga, N. Ise and T. Hashimoto, Langmuir 15 (1999) p.2684.

[26] F.J. Millero, Geochim. Cosmochim. Acta 59 (1995) p.661.

[27] S. Levine and G.H. Neal, J. Colloid Interface Sci. 47 (1974) p.520.

[28] P. Wette, H.-J. Schöpe, R. Biehl and T. Palberg, J. Chem. Phys. 114 (2001) p.7556.

[29] H.A. Wilson, Phil. Mag. 50 (1900) p.238.

[30] J. Frenkel, Phys. Z. Sowjetunion 1 (1932) p.498.

[31] (a) R. Wild and P. Harrowell, J. Chem. Phys. 114 (2001) p.9059; (b) R. Wild and P. Harrowell, Phys. Rev. E 56 (1997) p.3265.

[32] J.-P. Hansen and H. Löwen, Annu. Rev. Phys. Chem. 51 (2000) p.209.

[33] H. Löwen and G. Kramposthuber, Europhys. Lett. 23 (1993) p.637.

[34] H. Löwen and E. Allahyarov, J. Phys. Condens. Matter 10 (1998) p.4147.

[35] H. Löwen, T. Palberg and R. Simon, Phys. Rev. Lett. 70 (1993) p.1577.

[36] F. Bitzer, T. Palberg, H. Löwen, R. Simon and P. Leiderer, Phys. Rev. E 50 (1994) p.2821.

[37] P. Wette and H.J. Schöpe, Prog. Colloid Polym. Sci. 133 (2006) p.88.

[38] M.S. Ripoll, C.F. Tejero and M. Baus, Physica A 234 (1996) p.311.
[39] W. Luck, M. Klier and H. Wesslau, Naturwissenschaften 50 (1963) p.485.
[40] R. Messina and H. Löwen, Phys. Rev. E 73 (2006) p.011405.
[41] H. Löwen, R. Messina, N. Hoffmann, C.N. Likos, C. Eisenmann, P. Keim, U. Gasser, G. Maret, R. Goldberg and T. Palberg, J. Phys. Condens. Matter 17 (2005) p.S3379.
[42] A. Stipp, R. Biehl, Th. Preiss, J. Liu, A. Barreira Fontecha, H.J. Schöpe and T. Palberg, J. Phys. Condens. Matter 16 (2004) p.S3885.
[43] W.D. Dozier and P.M. Chaikin, J. Phys. France 43 (1982) p.843.
[44] P.M. Chaikin, J.M. diMeglio, W. Dozier, H.M. Lindsay and D.A. Weitz, in *Physics of Complex and Supramolecular Fluids*, S.A. Safran and N.A. Clark, eds., Wiley-Interscience, New York, 1987, p.6.